

---

# LOCALITY-CONSTRAINED AUTOREGRESSIVE CUM CONDITIONAL NORMALIZING FLOW FOR LATTICE FIELD THEORY SIMULATIONS

---

Dinesh P. R.\*

## ABSTRACT

Normalizing flow-based sampling methods have been successful in tackling computational challenges traditionally associated with simulating lattice quantum field theories. Further works have incorporated gauge and translational invariance of the action integral in the underlying neural networks, which have led to efficient training and inference in those models. In this paper, we incorporate locality of the action integral which leads to simplifications to the input domain of conditional normalizing flows that sample constant time sub-lattices in an autoregressive process, dubbed local-Autoregressive Conditional Normalizing Flow (l-ACNF). We find that the autocorrelation times of l-ACNF models outperform an equivalent normalizing flow model on the full lattice by orders of magnitude when sampling  $\phi^4$  theory on a 2 dimensional lattice.

## 1 Introduction

Solving path integrals in quantum field theories for theories with large couplings involves discretization of the underlying spacetime as lattice and numerically sampling the fields using Markov Chain Monte Carlo (MCMC) algorithms-referred to as lattice quantum field theory[9]. For large lattice sizes and choices of action parameters that lead to small lattice spacing and large correlation lengths, MCMC methods tend to suffer from long correlation times leading to exponentially diverging computational costs- a phenomenon known as critical slowing down (CSD)[17]. While a few non-local update algorithms have been developed for specific models to address CSD [13, 16], they cannot be applied for many key theories including quantum chromodynamics (QCD).

In recent times, machine learning-based methods [19, 18] have been explored for building generative models of statistical and field theories on a lattice. In particular, a technique based on training normalizing flows followed by independent Metropolis-Hastings sampling [2] was shown to nearly eliminate CSD while modelling the  $\phi^4$  theory in 2 dimensions. Subsequent works [7, 3] proposed ways of incorporate gauge invariance of the action integral when modelling gauge field theories using normalizing flows. This eliminated unnecessary degrees of freedom in the variational distribution modeled by the flow when local  $SU(N)$  symmetries are present and reducing computational costs of training and inference of the model. This addresses a well-known problem in machine learning traditionally known as the curse of dimensionality[8] where training time and model complexity are expected to increase exponentially with the size (dimensionality) of input/output data. Even though deep neural networks are shown to break this curse in many cases[11], this is only valid under approximation that the target function depends on low-dimensional projections of the input[4]. This is a pretty bad approximation for generative models of lattice field theories when correlation lengths are proportional to the lattice size, hence eliminating unnecessary degrees of freedom is of vital importance. Another study [6] explores several ways of tackling poor convergence in normalizing flows when the underlying distribution is multimodal- like in broken symmetry phases. It also introduces masked convolutional networks as conditional maps of coupling layers that enforce (broken) translational invariance and a notion of locality with stronger local dependence within the distribution.

In this work, we propose an autoregressive process of conditional normalizing flows which enforces locality of the action integral more strictly. By doing so, we reduce the effective input size of the conditional normalizing flow to  $O(L^{d-1})$  from the upper bound of  $L^d$ , hence further eliminating unnecessary degrees of freedom in the spirit

---

\*Project Associate, Indian Institute of Science Education and Research, Pune. Email: dinesh.pr@students.iiserpune.ac.in

of tackling the curse of dimensionality. We dub this *local-Autoregressive Conditional Normalizing Flow* (l-ACNF). After briefly introducing the system of interest and notations in sec. 2.1, we analyse the dependencies of autoregressive conditional distributions (introduced in sec. 2.2) in sec. 2.3 in fair detail. Sec. 2.4 discusses the mathematical structure of the l-ACNF model along with the accompanying Metropolis-Hamilton process. In sec. 3, we describe the numerical implementation for sampling the  $\phi^4$  theory in a 2D lattice using l-ACNF.

## 2 Mathematical background

### 2.1 Scalar lattice field theory

The system of interest consists of a hypercubic lattice of length  $L$  in  $d$  dimensions where every position is labeled using a  $d$ -dimensional vector  $\mathbf{r} \in [1, L]^d$ . For open boundary conditions, the lattice positions  $\mathbf{r} \notin [1, L]^d$  do not exist. In case of periodic boundary conditions, we map each component of  $\mathbf{r} \in \mathbb{Z}^d$  to  $r_i \rightarrow (r_i - 1) \bmod L + 1$ . State/configuration of the system is described using scalar field values  $\phi(\mathbf{r})$ . The configurations obey the Boltzmann distribution:

$$p(\phi(\mathbf{r})) = e^{-S[\phi]}/Z \quad (1)$$

where the *action*  $S[\phi]$  is a functional of the field  $\phi$  and  $Z$  is a normalizing constant known as partition function. For the scalar field theory with  $\phi^4$  interactions, the action is given by:

$$S[\phi] = \sum_{\mathbf{r} \in [1, L]^d} \left[ \phi(\mathbf{r}) \sum_{\bar{\mathbf{r}}} \square(\mathbf{r}, \bar{\mathbf{r}}) \phi(\bar{\mathbf{r}}) + m^2 \phi(\mathbf{r})^2 + \lambda \phi(\mathbf{r})^4 \right] \quad (2)$$

where  $m, \lambda$  are the bare mass and coupling. The d'Alembertian in the lattice approximation is given by:

$$\phi(\mathbf{r}) \sum_{\bar{\mathbf{r}}} \square(\mathbf{r}, \bar{\mathbf{r}}) \phi(\bar{\mathbf{r}}) = \sum_{\mu=1}^d 2\phi(\mathbf{r})^2 - \phi(\mathbf{r})\phi(\mathbf{r} - \hat{\mu}) - \phi(\mathbf{r})\phi(\mathbf{r} + \hat{\mu})$$

where  $\phi(\mathbf{r})$  can take any real value.

The action  $S[\phi]$  in 2 has many interesting mathematical properties. It contains only nearest neighbour product/interaction terms  $\phi(\mathbf{r})\phi(\mathbf{r} - \hat{\mu})$  and  $\phi(\mathbf{r})\phi(\mathbf{r} + \hat{\mu})$ , besides powers of  $\phi(\mathbf{r})$ . This makes the action *local*, a common feature in many fundamental physical theories. The action is also symmetric/invariant to the transformation  $\phi(\mathbf{r}) \rightarrow -\phi(\mathbf{r})$ , along with various discrete rotations and reflections of the lattice (hypercubic symmetry group).

### 2.2 Autoregressive process

The Boltzmann distribution in 1 depends on a large number of random variables  $L^d = N$  and it's usually difficult to sample from it or evaluate the PDF directly. One way to circumvent is to model it as a product of conditional distributions over individual random variables. Let's first replace the labels of lattice positions from vectors  $\mathbf{r} \in [1, L]^d$  to an integer *ordering*  $k \in [1, N]$ . We'll use a particular ordering that maps from vector labels as:

$$k(\mathbf{r}) = \left( \sum_{i=1}^d (r_i - 1)L^{i-1} \right) + 1 \quad (3)$$

Using a chain rule obtained from repeated application of Bayes theorem, we can decompose the probability into a product of  $N$  conditional probabilities, in the above ordering:

$$\begin{aligned} p(\{\phi_k | k \in [1, N]\}) &= p(\phi_1, \phi_2 \dots \phi_N) = p(\phi_1)p(\phi_2|\phi_1) \dots p(\phi_N|\phi_{N-1} \dots, \phi_1) \\ \implies \log p(\{\phi_k | k \in [1, N]\}) &= \log p(\phi_1) + \log p(\phi_2|\phi_1) + \dots \log p(\phi_N|\phi_{N-1} \dots, \phi_1) \end{aligned} \quad (4)$$

$$= \sum_{k \in [1, N]} \log p(\phi_k | \phi_{<k}) \quad (5)$$

This is referred to as an *autoregressive process*. If we can evaluate and sample the conditional probabilities sequentially, this would yield a sample and log-probability of the entire Boltzmann distribution. Exact forms of  $p(\phi_k | \phi_{<k})$  are still analytically intractable starting from 1. So approaches using this principle usually optimize the KL-divergence between a machine learning-based variational distribution and the unnormalized Boltzmann distribution[19].

### 2.3 $d - 1$ dimensional dependency sets for local interactions

**Ising model and open boundary conditions** Examining the  $k$ th conditional probability  $p(\phi_k|\phi_{<k})$  in 5, its distribution in general depends on  $k - 1$  values in  $\phi_{<k} = \{\phi_{k-1}, \dots, \phi_1\}$ . This means the complexity of these distributions can explode if the number of lattice points  $N$  is large, which is typically the case of interest. However for systems with nearest neighbour interactions, the *dependency set* is significantly smaller [12]. It's easier to show this (without loss of generality) for the nearest neighbour Ising model whose action is given by:

$$S[\phi] = -\beta J \sum_{\mu=1}^d \sum_{\mathbf{r}} \phi(\mathbf{r} - \hat{\mu})\phi(\mathbf{r}) \quad (6)$$

where  $\phi(\mathbf{x})$  takes values  $\pm 1$ . We'll assume *open* boundary conditions for now and relax it later on. Restating the Boltzmann distribution for the Ising model as an autoregressive process<sup>2</sup>:

$$\prod_{k=1}^N p(\phi_k|\phi_{<k}) = p(\phi) = \exp\left(-\beta J \sum_{\mu=1}^d \sum_k \phi_k \phi_{k-\hat{\mu}}\right) / Z \quad (7)$$

From Bayes theorem, we can relate this conditional probability to the unconditional joint probabilities of the first  $k$  and  $k - 1$  spins, which can in turn be written as integrated forms of the Boltzmann distribution:

$$p(\phi_k|\phi_{<k}) = \frac{p(\phi_1, \dots, \phi_k)}{p(\phi_1, \dots, \phi_{k-1})} = \frac{\sum_{\phi_{k+1} \dots \phi_N} p(\phi)}{\sum_{\phi_k \dots \phi_N} p(\phi)}$$

Expanding the  $p(\phi)$  for the Ising model:

$$p(\phi_k|\phi_{<k}) = \frac{\sum_{\phi_N, \dots, \phi_{k+1}} \exp\left(-\beta J \sum_{l=k}^N \left(\phi_l \sum_{\mu} \phi_{l-\hat{\mu}}\right) + \delta(\phi_{<k})\right)}{\sum_{\phi_N, \dots, \phi_k} \exp\left(-\beta J \sum_{l=k}^N \left(\phi_l \sum_{\mu} \phi_{l-\hat{\mu}}\right) + \delta(\phi_{<k})\right)}$$

Since the values in  $\phi_{<k}$  are fixed and not summed over, the terms  $\delta(\phi_{<k})$  containing only them cancel from both the numerator and denominator, leaving us with:

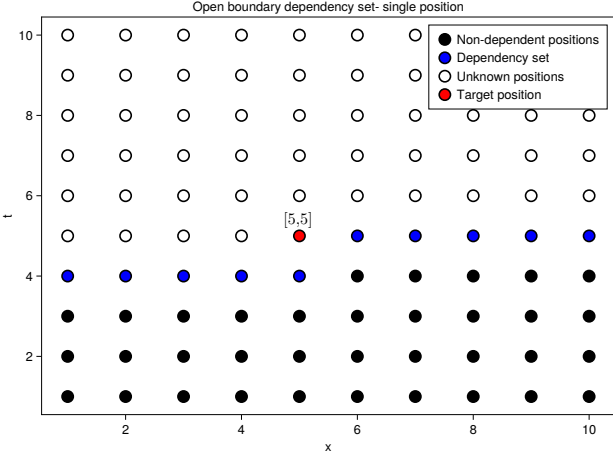
$$p(\phi_k|\phi_{<k}) = \frac{\sum_{\phi_N, \dots, \phi_{k+1}} \exp\left(-\beta J \sum_{l=k}^N \phi_l \sum_{\mu} \phi_{l-\hat{\mu}}\right)}{\sum_{\phi_N, \dots, \phi_k} \exp\left(-\beta J \sum_{l=k}^N \phi_l \sum_{\mu} \phi_{l-\hat{\mu}}\right)} \quad (8)$$

Even though  $\phi_{<k}$  contains  $k - 1$  values, the conditional probability  $p(\phi_k|\phi_{<k})$  depends only on those positions within  $\phi_{<k}$  that are nearest neighbours of the positions in  $\phi_{\geq k}$ . We can draw the same conclusion for scalar lattice field theory by replacing the sums with integrals and including terms like  $\phi_l^2$  and  $\phi_l^4$  in the above expression. The number of elements in the dependency set is bounded above by  $L^{d-1}$  or  $N/L$  for our choice of ordering (see figure 1a for an illustration on a  $10 \times 10$  2D lattice) which is orders of magnitude smaller than the original upper bound  $N$ . In fact, we can join the 2 strips of blue spins in figure 1a into a single 1D line of length  $L^{2-1} = 10$ , and the conditional distribution on  $\phi_k$  simply depends on the values along this line.

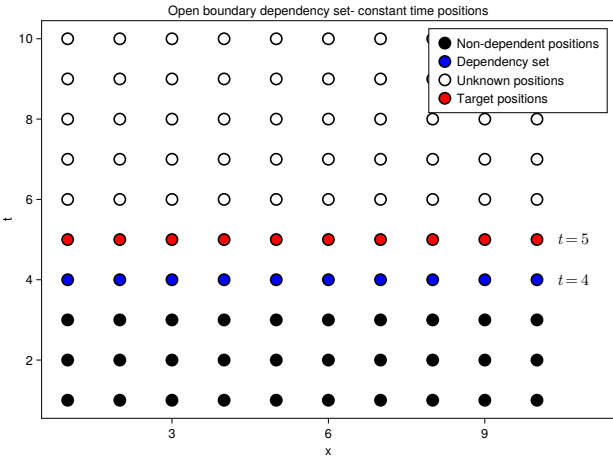
We can draw the same conclusion for scalar lattice field theory by replacing the sums with integrals and including terms like  $\phi_l^2$  and  $\phi_l^4$  in 8. Let's split the lattice vector  $\mathbf{r}$  into a  $d - 1$  dimensional *spatial* vector  $\mathbf{x} = [x_1, \dots, x_{d-1}]$  and *time*  $t$  so that  $\mathbf{r} = [r_1 = x_1, \dots, r_{d-1} = x_{d-1}, r_d = t]$ . In figure 1a for a  $10 \times 10$  lattice, the dependency set of blue positions is them simply a line of length  $L$  along the spatial dimension  $x$ . More generally, the dependency set of  $\phi_{k(\mathbf{r})}$  can be cast as a  $d - 1$  dimensional spatial sub-lattice that's defined parametrically using:

$$B_{\mathbf{r}}^o = \left\{ \mathbf{r}' | \mathbf{r}' = \begin{cases} [\mathbf{x}', t] & \text{if } k([\mathbf{x}', t]) < k(\mathbf{r}) \\ [\mathbf{x}', t - 1] & \text{if } k([\mathbf{x}', t]) > k(\mathbf{r}) \end{cases} \right\} \quad (9)$$

<sup>2</sup> $k - \hat{\mu}$  should be understood as the lattice position  $\mathbf{x} - \hat{\mu}$  where  $\mathbf{x}$  maps to  $k$  according to the given ordering



(a) The conditional probability  $p(\phi_k | \phi_{<k})$  of the field at red position depends only on the nearest neighbours of the positions in  $\phi_{\geq k}$  (coloured red/white). The dependency set consists only of blue positions while the black positions within  $\phi_{<k}$  can be ignored.



(b) The conditional probability of the field at red positions at a constant time  $p(\{\phi(x, t) | t = 5\} | \{\phi(x, t) | t < 5\})$  depends only on the positions with  $t = 4$  marked blue  $\{\phi(x, t) | t = 4\}$  and not the remaining ones marked black.

Figure 1: Dependency sets for the conditional probabilities of field value at single position (1a) and joint conditional probability of positions in a constant time manifold (1b), assuming open boundary conditions.

We'll call this the *dependency surface* at  $\mathbf{r}$ . From 8, we can write down the joint conditional probabilities for more than one variable. For example, we can write down this  $m$  variable joint distribution for the Ising model:

$$\begin{aligned} p(\{\phi_k, \dots, \phi_{k+m-1}\} | \phi_{<k}) &= p(\phi_k | \phi_{<k}) \dots p(\phi_{k+m-1} | \phi_{<k+m-1}) \\ &= \frac{\sum_{\phi_N, \dots, \phi_{k+m}} \exp\left(-\beta J \sum_{l=k}^N \left(\phi_l \sum_{\mu} \phi_{l-\hat{\mu}}\right)\right)}{\sum_{\phi_N, \dots, \phi_k} \exp\left(-\beta J \sum_{l=k}^N \left(\phi_l \sum_{\mu} \phi_{l-\hat{\mu}}\right)\right)} \end{aligned} \quad (10)$$

For the choice of  $\mathbf{r} = [1, \dots, 1, t]$  and  $m = L^{d-1}$ , the set  $\{\phi_k, \dots, \phi_{k+m-1}\}$  is the *constant time sub-lattice*  $\{\mathbf{r}' | t' = t\}$ , the dependency surface is the constant time manifold at the previous time step:

$$B_t^o = \{\mathbf{r}' | t' = t - 1\} \quad (11)$$

See figure 1b for an example in a  $10 \times 10$  lattice. This essentially reduces the overall autoregressive process to a first order Markov process in the time dimension.

**Periodic boundary conditions** The general observation that the dependency surface of  $\phi_{k(\mathbf{r})}$  contains only the nearest neighbours of  $\phi_{\geq k}$  within  $\phi_{<k}$  is true regardless of boundary conditions as long as the action is local. However, the dependency surface consists of two  $n - 1$  dimensional sub-lattices in case of periodic boundary conditions:

$$B_t^p = B_t^o \cup \{\mathbf{r} | r_d = 1\} \quad (12)$$

which includes the sub-lattice corresponding to the *initial time* sub-lattice. Note that periodic boundaries topologically renders the lattice as  $d$  dimensional torus, hence  $B_t^o = \{r_d = t - 1\}$  would be a  $d - 1$  torus along the spatial dimensions. This torus effectively ‘‘blocks’’ the influence of all equal time  $r_d < t$  tori except for the initial one  $r_d = 1$  which is connected to  $r_d > t$  on the other side. This is illustrated for  $d = 2$  in the figure 2. In other words, only the sub-lattices at  $r_d = t - 1$  and  $r_d = 1$  are *connected* to the sub-lattice  $r_d = t$  either directly or via unknown/future positions.

We'll assume periodic boundary conditions in our models since we can take advantage of the translational invariance of the action<sup>3</sup>.

## 2.4 Autoregressive Conditional Normalizing Flows and Metropolis sampling

### 2.4.1 Conditional masked normalizing flow

Conditional normalizing flow[15] models a bijective map  $f_\theta$  between samples of a standard prior distribution  $z \sim r(z)$  to samples of a variational distribution conditioned on  $\chi$ ,  $\tilde{\phi} \sim \tilde{q}_{f,\theta}(\tilde{\phi} | \chi)$ , so that  $\tilde{\phi} = f_\theta(z)$ . From the change of variables formula for probability distributions, we can obtain the log PDF of the variational distribution:

$$\begin{aligned} \log r(z) &= \log \tilde{q}_{f,\theta}(f_\theta(z) | \chi) + \log \left| \det \frac{\partial f_\theta(z)}{\partial z} \right| \\ \Rightarrow \log \tilde{q}_{f,\theta}(f_\theta(z) | \chi) &= \log r(z) - \log \left| \det \frac{\partial f_\theta(z)}{\partial z} \right| \end{aligned} \quad (13)$$

The map  $f_\theta$  is constructed using a sequence of  $n$  coupling layers  $g^{(i)}$  whose inputs are acted alternatively by complementary binary masks  $m$  and  $1 - m$ <sup>4</sup>:

$$\begin{aligned} f_\theta(z) &= (g_1 \circ \dots \circ g_n)(z) \\ g_i(z_i, \chi) &= m^{(i)}(z_i) + (1 - m^{(i)}) \left( \tilde{\phi} e^{s^{(i)}(m^{(i)}(z_i), \chi)} + t^{(i)}(m^{(i)}(z_i), \chi) \right) \\ m^{(i)} &= \begin{cases} m & i \text{ even} \\ 1 - m & i \text{ odd} \end{cases} \end{aligned} \quad (14)$$

<sup>3</sup>Circular permutation invariance is the accurate description for finite lattices with periodic boundary condition, while true translational invariance strictly occurs only for an infinite lattice.

<sup>4</sup>All products are element-wise unless stated otherwise

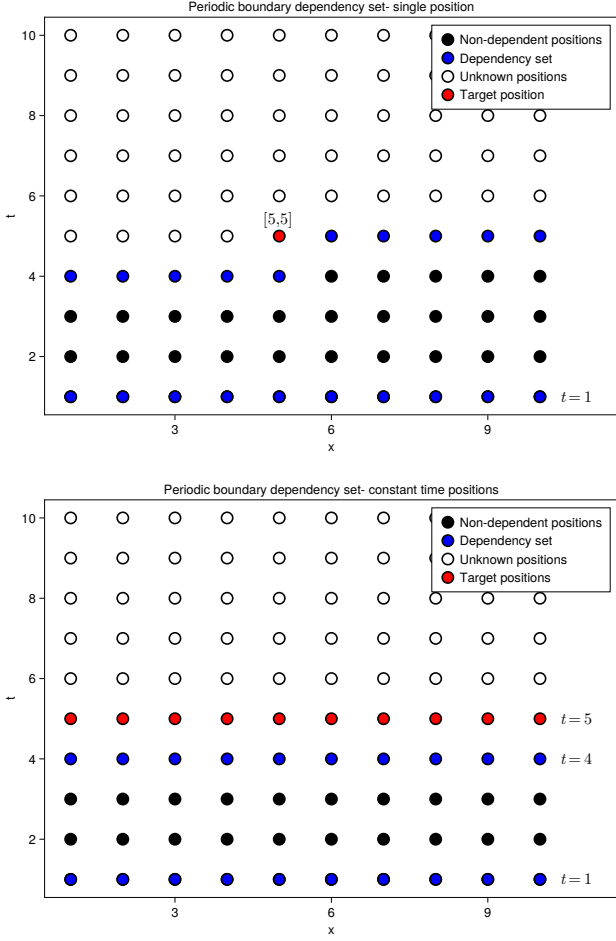


Figure 2: In case of a periodic boundary, distributions of field values at a single red position (top) or positions in a constant time sub-lattice (bottom) are conditioned on the dependency sets (marked blue) that are similar to that of an open boundary, but including the initial time sub-lattice at  $t = 1$ .

where  $z_1 = z$  and  $z_i = g_{i-1}(z_{i-1}, \chi)$  for  $i > 1$ , so  $z_{n+1} = \tilde{\phi}$ . The functions  $s^{(i)}$  and  $t^{(i)}$  are in turn modeled using feed-forward neural networks. The log determinant in 13 then becomes:

$$\log \left| \det \frac{\partial f_{\theta}(z)}{\partial z} \right| = \sum_{i=1}^n \log \left| \det \frac{\partial g_i(z_i)}{\partial z_i} \right| = \sum_{i=1}^n \text{sum}(s^{(i)}(m^{(i)}(z_i), \chi))$$

where the sum function adds up an input array of values. The couplings can be inverted and composed together for the inverse flow:

$$g_i^{-1}(z_{i+1}, \chi) = m^{(i)}(z_{i+1}) + (1 - m^{(i)}) \left( z_{i+1} + t^{(i)}(m^{(i)}(z_{i+1}), \chi) \right) e^{-s^{(i)}(m^{(i)}(z_{i+1}), \chi)}$$

$$f_{\theta}^{-1}(\tilde{\phi}) = (g_n^{-1} \circ \dots \circ g_1^{-1})(\tilde{\phi}) \quad (15)$$

which is useful to evaluate the log PDF of a known sample  $\tilde{\phi}$  of the variational distribution:

$$\log \tilde{q}_{f, \theta}(\tilde{\phi} | \chi) = \log r(f_{\theta}^{-1}(\tilde{\phi})) - \sum_{i=1}^n \text{sum}(s^{(i)}(m^{(i)}(z_{i+1}), \chi)) \quad (16)$$

## 2.4.2 Autoregressive process

We split the Boltzmann distribution as a product of conditional distributions of the field at single positions in 5. We then generalized this and evaluated the dependency sets for joint conditional distribution of the field values in a constant

time sub-lattice in 11. Let’s rewrite this joint conditional distribution for periodic boundary conditions, but this time conditioned on the coupling  $\lambda$  in 2 as well:

$$p(\{\phi(\mathbf{r})|t\}|\phi_{<[1,\dots,t]}, \lambda) = p(\{\phi(\mathbf{r})|t\}|\{\phi(\mathbf{r}')|t' = t - 1, 1\} \cup \lambda)$$

$$\implies \log p(\phi|\lambda) = \sum_{t=1}^L \log p(\{\phi(\mathbf{r})|x_d = t\}|\{\phi(\mathbf{r})|x_d = t - 1, 1\} \cup \lambda)$$

where the second line is the full Boltzmann distribution in logarithmic form. We use the output variational distribution from a conditional normalizing flow  $\tilde{q}_\theta(\tilde{\phi}|\chi, t)$  to model the individual conditional distributions in the RHS, where  $\chi = \{\phi(\mathbf{r})|x_d = t - 1, 1\} \cup \lambda$ . We sample one constant time manifold of  $\tilde{\phi}(t) = \{\phi(\mathbf{r})|x_d = t\}$  at a time and supply them as inputs to subsequent calls of the normalizing flow:

$$\begin{aligned} \tilde{\phi}(1) &\sim \tilde{q}_\theta(\tilde{\phi}|\Theta, \Theta, \lambda, 1) = \tilde{q}_\theta(1) \\ &\vdots \\ \tilde{\phi}(k) &\sim \tilde{q}_\theta(\tilde{\phi}|\tilde{\phi}(k-1), \tilde{\phi}(1), \lambda, k) = \tilde{q}_\theta(k) \\ &\vdots \\ \tilde{\phi}(L) &\sim \tilde{q}_\theta(\tilde{\phi}|\tilde{\phi}(L-1), \tilde{\phi}(1), \lambda, L) = \tilde{q}_\theta(L) \end{aligned} \tag{17}$$

where  $\theta$  are neural network weights and  $\Theta$  are junk/missing values<sup>5</sup>. Note that we explicitly supply time as an input since the conditional distributions aren’t necessarily time independent/invariant. Finally, we can concatenate the samples along the time direction and add the log PDFs to obtain the sample and corresponding log PDF of the final model distribution  $q_\theta(\phi)$  of 1-ACNF:

$$\begin{aligned} \phi &= \text{cat}_{t=1}^L \tilde{\phi}(t) \\ \log q_\theta(\phi) &= \sum_{t=1}^L \log \tilde{q}_\theta(t) \end{aligned}$$

We optimize the weights  $\theta$  such that the KL-divergence between the distributions  $q_\theta$  and  $p$  is minimized:

$$\begin{aligned} \text{KL}(p||q_\theta) &= \mathbb{E}_{q_\theta(\phi)} [\log q_\theta(\phi) - \log p(\phi)] \\ &= \frac{1}{M} \sum_{i=1}^M [\log q_\theta(\phi^{(i)}) + S[\phi^{(i)}]] \quad \phi^{(i)} \in \{\phi \sim q_\theta\}^M \end{aligned} \tag{18}$$

where we sample mini-batches of  $\phi$  (of size  $M$ ), evaluate the mean of the quantity in square brackets and use the gradient of this quantity wrt  $\theta$  to update the weights at every step. We ignore the log of partition function  $\log Z$  in the expansion of  $\log p(\phi)$  since it’s a constant independent of  $\phi$ .

### 2.4.3 Checkerboard masks and convolutional networks

Particular choices of neural network architecture for  $s^{(i)}$  and  $t^{(i)}$ , and the binary mask  $m$  used in 14 have algorithmic benefits in the context of generative modeling of the scalar lattice field theory. Neural networks containing only  $d - 1$  dimensional convolutional layers with circular padding (along with activations and residual connections) and checkerboard mask for  $m$  enable a broken translational invariance along the  $d - 1$  spatial dimensions of the lattice[6] (as long as it’s a symmetry of the prior distribution  $r(z)$  in 13). No such invariances exist explicitly along the time dimension since we sequentially sample along this direction, though a well-trained model is expected to approximately satisfy them. Fully convolutional networks also enable sampling configurations independent of the lattice size  $L$  along the spatial dimensions. Autoregressive sampling in 17 features dependency sets independent of  $L$  along the time dimension, hence we can sample lattices of different sizes compared to the  $L$  that was used to train the model- making it *scalable*.  $L$  is still constrained to be an even integer in order to avoid “leaks” in the normalizing flow due to checkerboard masks.

For benchmarking our model, we also consider a masked normalizing flow with  $d$  dimensional convolutional layers and circular padding where the NF generates entire lattice configurations (instead of constant time sub-lattices) conditioned only on the coupling  $\lambda$ , similar to the implementation described in [6]. This admits translational invariance along all  $d$  directions and scalable as well. 1-ACNF has the (theoretical) advantage of better tackling the *curse of dimensionality* with smaller effective input size ( $O(L^{d-1})$ ) compared to the latter ( $L^d$ ).

<sup>5</sup>We supply zero fields along with a boolean flag for the initial sampling. See code implementation for details.

### 2.4.4 Metropolis-Hastings sampling

Any bias in the variational distribution after training to minimize the KL-divergence in 18 results in bias for various observables/estimators evaluated after sampling from it. To get unbiased samples of  $p$  from  $q_\theta$ , we run its samples through a Metropolis-Hastings procedure- a Markov Chain Monte Carlo (MCMC) technique. Starting from an initial sample  $\phi^{(1)}$  and corresponding log PDF  $\log q_\theta(\phi^{(1)})$ , we update the chain in the  $i$ th step using current sample  $\phi^{(i)}$  and the proposed sample  $\phi'$  using:

$$\begin{aligned} A(\phi^{(i-1)}, \phi') &= \min \left( 1, \exp \left( \log q_\theta(\phi^{(i-1)}) - \log p(\phi^{(i-1)}) - \log q_\theta(\phi') + \log p(\phi') \right) \right) \\ &= \min \left( 1, \exp \left( \log q_\theta(\phi^{(i-1)}) - S[\phi^{(i-1)}] - \log q_\theta(\phi') + S[\phi'] \right) \right) \\ \phi^{(i)} &= \begin{cases} \phi' & A < \pi \\ \phi & \text{else} \end{cases} \quad \text{where } \pi \sim \text{Uniform}(0, 1) \end{aligned} \quad (19)$$

A necessary condition for the asymptotic convergence of Metropolis-Hastings samples to  $p$  is *ergodicity* which requires:

$$q_\theta(\phi) > 0 \quad \text{or} \quad \log q_\theta(\phi) > -\infty \quad \forall \phi \in \mathbb{R}^{L^d}$$

The normalizing flow in  $q_\theta$  satisfies this condition if the prior distribution of the flow satisfies  $r(z) > 0 \forall z \in \mathbb{R}$  which is true in case of a Gaussian prior, for example.

### 2.4.5 Symmetrizing and adiabatic retraining

In the Metropolis-Hastings update step 19, it's useful to ensure various symmetry transformations of the proposed configuration (that render the action  $S$  invariant) leave the acceptance probability  $A$  unchanged. This includes translations and reflections of the lattice, translations along every dimension and the negation  $\phi \rightarrow -\phi$ . This amounts to averaging over the PDF  $\text{Avg}_{\mathfrak{g}} q_\theta(\mathfrak{g}(\phi))$  after applying the transformations  $\mathfrak{g}$  and choosing a randomly transformed field at every step  $\mathfrak{g}(\phi)$ :

$$\begin{aligned} \log q_\theta(\phi) &\rightarrow \log \text{sumexp}_{\mathfrak{g} \in G} (\log q_\theta(\mathfrak{g}(\phi))) - \log |G| \\ \phi &\rightarrow \mathfrak{g}(\phi) \quad \mathfrak{g} \sim G \end{aligned} \quad (20)$$

where  $G$  is the set of all symmetry transformations we consider. This is one way of tackling poor convergence when the distribution  $p(\phi)$  has well-separated modes as studied in [6]. In our case, rotations between the time and spatial dimensions also address the inherent asymmetrical treatment between spatial and time dimensions as well as lack of invariances along time dimension in l-ACNF, as mentioned in 2.4.3. The scalability of the model to sample lattice sizes different from the value it trained on allows us to perform adiabatic retraining- where we initially train with smaller  $L$  and use this network as an initial state for training larger  $L$ , similar to [3].

## 3 Numerical experiments

### 3.1 Network architecture and training

The python deep learning library Pytorch[10] was used to build all models used in this study. We model the  $\phi^4$  theory in a 2 dimensional lattice ( $d = 2$ ) with length 16 ( $L = 16$ ). For Model 1, the conditional normalizing flow network contains  $n = 8$  coupling layers described in 14. As mentioned in 2.4.3, we use 1D checkerboard binary masks  $m$  and 1D gated convolutional networks[14] for the functions  $s^{(i)}$  and  $t^{(i)}$ , where the conditional variables  $\chi$  are processed by a common chain of 4 gated-convolutional networks and passed as a skip connection to another gated-convolutional network with input  $m^{(i)} z_i$ . The model is trained using the KL-divergence loss in 18 after setting  $m^2 = -4$  and  $\lambda \sim \text{Uniform}(4.8, 5.4)$  is sampled at every step- for 9000 steps using Adam optimizer and learning rate  $\eta = 10^{-3}$  with Step schedule for  $\approx 90$  minutes. Model 2 was constructed by adiabatic-retraining Model 1, with  $L = 20$  for  $\approx 40$  minutes using  $\eta = 10^{-5}$  with the same optimizer and schedule. Model 3 is constructed using a 2D masked normalizing flow as described in the second paragraph of 2.4.3 for benchmarking Model 1. It uses 2D checkerboard masks and 2D gated convolutional networks with circular padding for  $n = 12$  coupling layers. This ensures equal number of convolutional operations and non-linear activations across all models, with slightly higher number of weights due to 2D convolutional layers. Model 3 was trained with  $L = 16$  for  $\approx 90$  minutes using  $\eta = 10^{-3}$  to maintain equivalence with Model 1.

All training and inference was done using an Nvidia RTX 2060 mobile GPU. Source code is available at <https://github.com/dinesh110598/l-ACNF-scalar>. The data and code for all plots is available in an interactive Julia notebook here: <https://github.com/dinesh110598/l-ACNF-scalar/blob/main/Figures/notebook.jl>.



$L$	8	10	12	14	16	18	20
$\lambda$	6.008	5.550	5.276	5.113	4.99	4.89	4.82

Table 1: Couplings  $\lambda$  corresponding to  $L \leq 14$  were used in a previous study so that the system lies along the  $m_p L \approx 4$  critical line. Values for  $L \geq 16$  were determined by trial and error evaluations of  $m_p L$  for different  $\lambda$  using our model. See figure 3 for a plot of  $m_p L$  vs  $L$  at these values of  $\lambda$ .

### 3.2 Parameters and observables

The parameters  $m^2$  and  $\lambda$  in 2 were chosen close to the  $m_p L \approx 4$  critical line at the symmetrical phase of the system, similar to the study in [2]. The difference is we use a single trained model to evaluate all observables at different lattice lengths  $L$  and couplings  $\lambda$ . Observables of interest include the 2-point Green's function:

$$G_c(\mathbf{r}) = \frac{1}{N} \sum_{\mathbf{r}'} (\langle \phi(\mathbf{r}') \phi(\mathbf{r}' + \mathbf{r}) \rangle - \langle \phi(\mathbf{r}') \rangle \langle \phi(\mathbf{r}' + \mathbf{r}) \rangle)$$

its spatial fourier transform

$$\tilde{G}_c(\mathbf{p}, t) = \frac{1}{L^{d-1}} \sum_{\mathbf{x}} e^{i\mathbf{p} \cdot \mathbf{x}} G_c(\mathbf{x}, t)$$

an estimator of pole mass

$$m_p(t) = \operatorname{arccosh} \left( \frac{\tilde{G}_c(0, t-1) + \tilde{G}_c(0, t+1)}{2\tilde{G}_c(0, t)} \right) \quad (21)$$

the 2-point susceptibility

$$\chi_2 = \sum_{\mathbf{r}} G_c(\mathbf{r})$$

and the average Ising energy density

$$E = \frac{1}{d} \sum_{\mu=1}^d G_c(\hat{\mu})$$

We also study an autocorrelation function based on the accept/reject statistics of the Metropolis-Hastings chain of length  $T$ :

$$\rho(\tau)/\rho(0)_{acc} = \frac{1}{T-\tau} \sum_{j=1}^{T-\tau} \prod_{i=1}^{\tau} \mathbf{1}_{rej}(i+j) \quad (22)$$

where  $\mathbf{1}_{rej}$  is the identity map of a rejected MH step. Another set of estimators of the autocorrelation is based on the 2-point observables we defined above

$$\rho(\tau)/\rho(0)_{\mathcal{O}} = \frac{\frac{1}{T-\tau} \sum_{i=1}^{T-\tau} (\mathcal{O}_i - \bar{\mathcal{O}})(\mathcal{O}_{i+\tau} - \bar{\mathcal{O}})}{\frac{1}{T} \sum_{i=1}^T (\mathcal{O}_i - \bar{\mathcal{O}})^2} \quad (23)$$

The integrated autocorrelation time wrt acceptance statistics is given by

$$\tau_{acc}^{int} = \frac{1}{2} + \lim_{\tau_{max} \rightarrow \infty} \sum_{\tau=1}^{\tau_{max}} \frac{\rho_{acc}(\tau)}{\rho_{acc}(0)} \approx \frac{1}{2} + \lim_{\tau_{max} \rightarrow \infty} \sum_{\tau=1}^{\tau_{max}} \rho(\tau)/\rho(0)_{acc} \quad (24)$$

and the dynamical critical exponent  $z$  for the above quantity is fit using

$$\tau_{acc}^{int}(L) \approx cL^z \quad (25)$$

We set  $T = 10^5$  and  $L \in [8, 10, 12, 14, 16, 18, 20]$ . In every Metropolis-Hastings step given by 19, symmetrization in 20 was done to transform  $\phi^{(i)}$  and  $\log q_{\theta}(\phi^{(i)})$  after every ( $i$ th) step. While this lead to a slower MCMC evaluation, it significantly improved rates from between 50-55% to 65-70%. In table 1, we list the values of  $\lambda$  used in [2] for  $L \leq 14$  and the remaining fit by trial and error using Model 1 from 21. Figure 3 has a plot of  $m_p L$  vs  $L$  at the specified  $\lambda$  and the points are close to the red-dashed critical line at these points. Autocorrelation functions wrt acceptance/rejection statistics (Model 1) and the observables  $G_c(0), \chi_2, E$  are plotted based on 22 and 23 in figure 4. The orange and red curves corresponding to  $L = 18, 20$  seem to decrease slowly in comparison to others. In the plot integrated autocorrelation times in figure 5, we evaluate  $\tau_{acc}^{int}$  from 24 against  $L$  using all of models 1, 2 and 3. The most striking

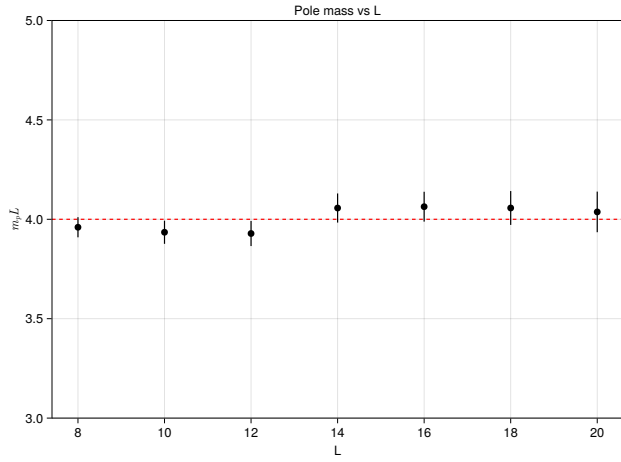


Figure 3: Product of pole mass and lattice length  $m_p L$  plotted against  $L$  evaluated using Model 1. Error bars indicate 68% confidence intervals obtained from moving block bootstrap resampling with block size 100

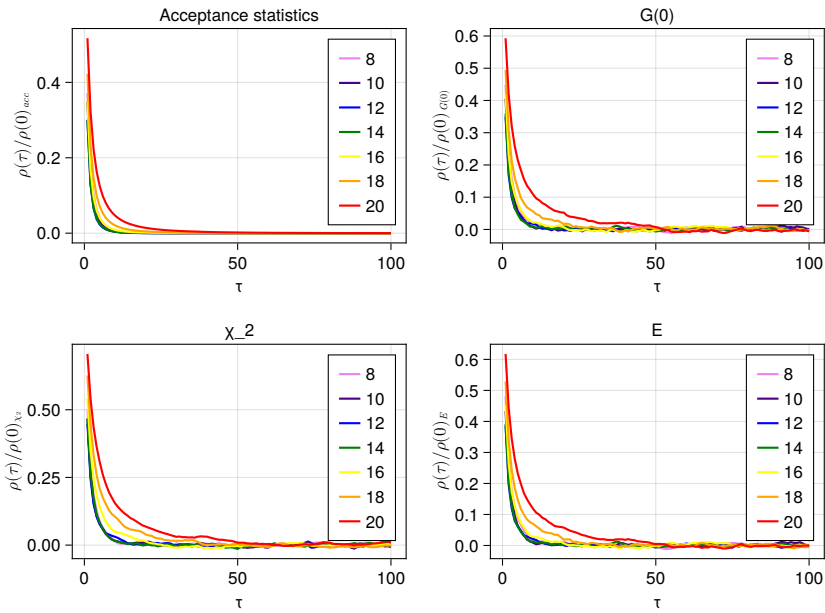


Figure 4: Plots of the autocorrelation functions wrt acceptance statistics and different observables at various lattice lengths evaluated using Model 1

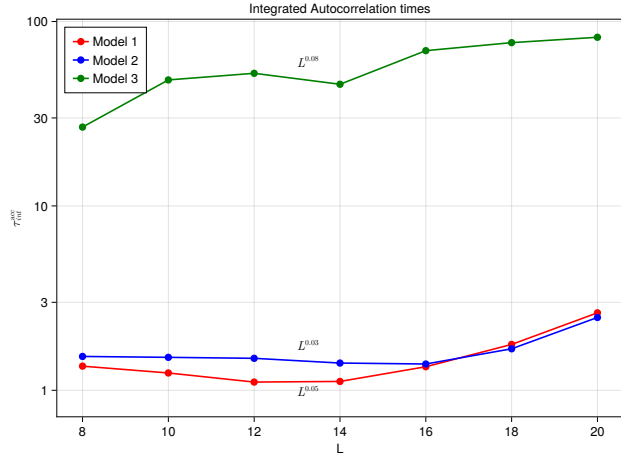


Figure 5: Integrated autocorrelation times for acceptance statistics plotted against  $L$  in the logarithm scale using Model 1, 2 and 3

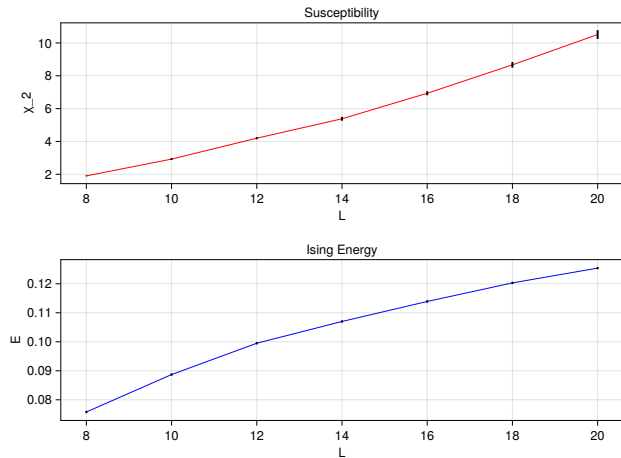


Figure 6: Plot of observables  $\chi_2$  and  $E$  against  $L$  using Model 1. The error bars indicate 95% confidence intervals obtained from moving block bootstrap resampling with block size 100

feature in this plot is that the green line representing the autocorrelation times of model 3 has values that are orders of magnitude larger than that of models 1,2 which autoregressively sample constant time sub-lattices according to our proposal. The values for the adiabatically-retrained model 2 in the blue line is flatter and has a smaller dynamical critical exponent compared to that model 1 represented by the red line. The autocorrelation times generally remain roughly constant between  $L = 8$  and  $L = 14$  and increase between  $L = 16$  and  $L = 20$ , suggesting that the quality (in terms of closeness to the actual Boltzmann distribution  $p$ ) of  $q_\theta$  drops when sampling lattice sizes larger than the value  $L = 16$  it was trained on. This could also be the reason for growing error bars above  $L = 16$  of the susceptibility plot (Model 1) in figure 6 as well as for the pole masses in figure 3. Still, the dynamical critical exponents obtained by fitting with the curve in 25 are close to zero, which is usually not the case with traditional methods<sup>6</sup>.

## 4 Concluding remarks

In this work, we proposed a generative model (dubbed l-ACNF) that autoregressively samples “equal-time” sub-lattices of a scalar lattice field using masked conditional normalizing flows. From the locality of action  $S$  for the  $\phi^4$  theory

<sup>6</sup>The scaling behavior of flow-based models usually depends on specific details of the implementation and curve-fitting to an exponential function can be inaccurate which is evident from the lack of straight-line behavior in our log-scale plots as well. See the study in [1] for more details.

in 2, we determined that these normalizing flows are conditioned on a smaller sub-lattice of size  $O(L^{d-1})$  according to 12 instead of the generic upper bound,  $L^d$ . In other words, locality of the action reduces the autoregressive expansion of the Boltzmann distribution to a Markov process in time. Models constructed according to our proposal have reported orders of magnitude smaller autocorrelation times compared to an equivalently-constructed existing model used in a previous study in [6]. This is a consequence of smaller input/output space for the conditional normalizing flows in our model, essentially addressing the curse of dimensionality in existing approaches- avoiding exponentially higher number of training epochs and/or using bulkier neural networks. Constraints in computing resources limited our study to models that train and converge within hours on relatively modest hardware. Yet, our models achieve small autocorrelation times and near-zero dynamic critical exponents similar to large-scale studies like [2]. If we're working with the true space-time specification of  $d = 4$ , l-ACNF uses 3D convolutions for sampling constant time sub-lattices instead of 4D convolutions. When running on GPU devices, the CUDNN library[5] (used by any deep learning framework to access GPU-optimized functions/methods) contains optimized convolution kernels for only upto 3 dimensions due to their relative practical utility, which offers a slight edge to l-ANF over alternatives.

Since locality is a generic property of all lattice quantum field theories, our approach can be extended to more complex theories as well. For example, the Wilson action for lattice gauge fields

$$S_W = - \sum_p \frac{2}{g^2} \text{Re}(\text{Tr}(U(p)))$$

is a sum over plaquettes  $p$  which are loops of links  $U_\mu(\mathbf{r})$  through nearest neighbours at every position  $\mathbf{r} = [\mathbf{x}, t]$  and along the direction  $\mu$ . We can extend the analysis in section 2.3 and determine that the conditional distribution of links on the equal-time sub-lattice  $p(\{U_\mu(\mathbf{r})|r_d = t\}|\{U_\mu(\mathbf{r})|r_d < t\})$  has the dependency set given by (assuming periodic boundary conditions):

$$B(\mathbf{r}|r_d = t) = \{U_\mu(\mathbf{r})|r_d = t - 1, \mu < d\} \cup \{U_\mu(\mathbf{r})|r_d = 1\}$$

which contains links inside the  $r_d = t - 1$  sub-lattice (except along the time dimension since they are not part of/connected to plaquettes containing links along  $t = t_o$ ) and the  $r_d = 1$  sub-lattice, which again reduces the input size of the corresponding flow networks to  $O(L^{d-1})$ . Combining our approach with gauge equivariant flows proposed in [7] and [3] is an interesting direction to investigate from here, but is unfortunately beyond the scope of this study.

## References

- [1] Ryan Abbott et al. "Aspects of scaling and scalability for flow-based sampling of lattice QCD". In: *arXiv preprint arXiv:2211.07541* (2022).
- [2] Michael S Albergo, Gurtej Kanwar, and Phiala E Shanahan. "Flow-based generative models for Markov chain Monte Carlo in lattice field theory". In: *Physical Review D* 100.3 (2019), p. 034515.
- [3] Denis Boyda et al. "Sampling using SU (N) gauge equivariant flows". In: *Physical Review D* 103.7 (2021), p. 074504.
- [4] Michael M Bronstein et al. "Geometric deep learning: Grids, groups, graphs, geodesics, and gauges". In: *arXiv preprint arXiv:2104.13478* (2021).
- [5] Sharan Chetlur et al. "cudnn: Efficient primitives for deep learning". In: *arXiv preprint arXiv:1410.0759* (2014).
- [6] Daniel C Hackett et al. "Flow-based sampling for multimodal distributions in lattice field theory". In: *arXiv preprint arXiv:2107.00734* (2021).
- [7] Gurtej Kanwar et al. "Equivariant flow-based sampling for lattice gauge theory". In: *Physical Review Letters* 125.12 (2020), p. 121601.
- [8] Mario Köppen. "The curse of dimensionality". In: *5th online world conference on soft computing in industrial applications (WSC5)*. Vol. 1. 2000, pp. 4–8.
- [9] Colin Morningstar. "The Monte Carlo method in quantum field theory". In: *arXiv preprint hep-lat/0702020* (2007).
- [10] Adam Paszke et al. "Pytorch: An imperative style, high-performance deep learning library". In: *Advances in neural information processing systems* 32 (2019).
- [11] Tomaso Poggio et al. "Why and when can deep-but not shallow-networks avoid the curse of dimensionality: a review". In: *International Journal of Automation and Computing* 14.5 (2017), pp. 503–519.
- [12] Dinesh PR. *Analysis of Ising model using neural networks*. July 2021. URL: <http://dr.iiserpune.ac.in:8080/xmlui/handle/123456789/6014>.
- [13] Robert H Swendsen and Jian-Sheng Wang. "Nonuniversal critical dynamics in Monte Carlo simulations". In: *Physical review letters* 58.2 (1987), p. 86.

- [14] Aaron Van den Oord et al. “Conditional image generation with pixelcnn decoders”. In: *Advances in neural information processing systems* 29 (2016).
- [15] Christina Winkler et al. “Learning likelihoods with conditional normalizing flows”. In: *arXiv preprint arXiv:1912.00042* (2019).
- [16] Ulli Wolff. “Collective Monte Carlo updating for spin systems”. In: *Physical Review Letters* 62.4 (1989), p. 361.
- [17] Ulli Wolff. “Critical slowing down”. In: *Nuclear Physics B-Proceedings Supplements* 17 (1990), pp. 93–102.
- [18] Dian Wu, Riccardo Rossi, and Giuseppe Carleo. “Unbiased Monte Carlo cluster updates with autoregressive neural networks”. In: *Physical Review Research* 3.4 (2021), p. L042024.
- [19] Dian Wu, Lei Wang, and Pan Zhang. “Solving statistical mechanics using variational autoregressive networks”. In: *Physical review letters* 122.8 (2019), p. 080602.